PAPER

A Schiff base platform: structures, sensing of Zn(II) and PPi in aqueous medium and anticancer activity†

Barnali Naskar,[a] Ritwik Modak,[a] Dilip K. Maiti,[a] Michael G. B. Drew,[b] Antonio Bauzá,[c] Antonio Frontera, [c] Chitrangada Das Mukhopadhyay,[d] Snehasis Mishra,[e] Krishna Das Saha[e] and Sanchita Goswami *[a]

A reaction of N_1,N_3-bis(3-methoxysalicylidene) diethylenetriamine (**H₂Vd**) and Zn(NO₃)₂·6H₂O, ZnBr₂, ZnI₂ and Cd(NO₃)₂·4H₂O in a methanol solution led to zinc and cadmium complexes of different nuclearities, [Zn₂(Vd·H)₂(X)₂]·CH₃OH (X = NO₃, Br, I) [**1a**, **1b** and **1c**] and Cd₃(Vd)₂(NO₃)₂ (**2**). In **1(a–c)**, two **H₂Vd** ligands bridge the two metal centers whereas in **2**, they provide sideways support to two terminal Cd^{2+} ions, providing an all-oxygen envelope to the central Cd^{2+} ion. All four compounds were characterized by elemental analysis, FT-IR spectroscopy and single crystal X-ray diffraction analysis. Complexes **1(a–c)** exhibit dinuclear structures, whereas **2** exhibits a nearly linear trinuclear structure. The structural differences among these complexes are attributable to various coordination modes and flexible configurations of the **H₂Vd** ligand. The ligand **H₂Vd** is an excellent probe for sensing Zn^{2+} in solution, whereas complexes **1(a–c)** are able to selectively detect pyrophosphate (PPi) in aqueous medium. The structure of the pyrophosphate (PPi) complex has been proposed using DFT calculations and the selectivity is due to the unique ability of this anion to simultaneously coordinate to both the Zn metal centers. The anticancer activity of complexes **1(a–c)** was also explored.

1. Introduction

Over the last century, the design and synthesis of metal–organic complexes have attracted tremendous attention not only for their attractive structures and topological networks[1] but also for their potential applications in luminescence,[2] chemical sensors[3] and so on. Vanillin based nitrogen rich Schiff bases bear an excellent coordinating ability to act as either multidentate ligands or bridging blocks in supramolecular chemistry and have been highlighted in the literature owing to the novel structural architectures and potential applications of their complexes.[4] With the above consideration in mind, we have ventured to explore the ligand N_1,N_3-bis(3-methoxysalicylidene) diethylenetriamine (**H₂Vd**) from the structural aspects of its zinc and cadmium coordination complexes and searched for potential applications.

Among the many biologically significant metal ions, Zn^{2+} is the second most abundant metal ion in the human body as it is involved in a number of biochemical processes.[5] However, both its deficiency and excess can induce human health problems in the form of Alzheimer's disease, Parkinson's disease *etc*.[6] Therefore, the generation of efficient chemosensors specific for Zn^{2+} detection is an important scientific challenge. Analytical methods for detection of Zn^{2+} such as atomic absorption spectrometry,[7] inductively coupled plasma mass spectroscopy (ICPMS),[8] inductively coupled plasma-atomic emission spectrometry (ICPAES),[9] and voltammetry[10] require expensive instrumentation and large amounts of samples. As a result, over the past few decades, fluorescence based chemosensors have been extremely useful[11] due to high sensitivity, easy visualization, and short response time for detection and most importantly they can be implemented for real time bioimaging.[12]

[a]*Department of Chemistry, University of Calcutta, 92, A.P.C. Road, Kolkata, India. E-mail: sgchem@caluniv.ac.in*
[b]*Department of Chemistry, University of Reading, Whiteknights, Reading RG6 6AD, UK*
[c]*Departament de Química, Universitat de les IllesBalears, Crta. deValldemossa km 7.5, 07122 Palma de Mallorca, Baleares, Spain*
[d]*Centre for Healthcare Science & Technology, Indian Institute of Engineering Science and Technology, Shibpur Howrah 711103, India*
[e]*Cancer and Inflammatory Disorder Division, CSIR-Indian Institute of Chemical Biology, Jadavpur, Kolkata 700032, West Bengal, India. E-mail: krishna@iicb.res.in*

Binding and sensing of phosphorylated substrates with high selectivity in solution is one of the greatest challenges of chemistry.[13] Among them, pyrophosphate (PPi) has been one of the most pursued targets because it is linked to numerous biological processes, such as energy storage, signal transduction, DNA/RNA polymerization, muscle contraction *etc.*[14,15] Therefore, recent research has focused on the detection and discrimination of pyrophosphate by means of fluorescent and colorimetric chemosensors.[16] However, so far, only a few chemical sensors have been found to detect PPi under physiological conditions in aqueous medium.[17] Several dinuclear metal complexes have been shown to display high affinity towards PPi owing to their ability to bind to PPi in a bridging manner.[18]

In this report, we have described the structural features of Zn^{2+} and Cd^{2+} coordination complexes of **H₂Vd**. At the same time, **H₂Vd** serves as a reliable sensor for Zn^{2+} at pH 7.4 in solution as well as in HCT cells with detection limit in the nanomolar range. The generated **H₂Vd**-Zn^{2+} ensemble turned out to be an efficient sensor for PPi in aqueous solution. Again, the zinc complex exhibits promising anticancer activity when tested on HCT 116 cells. Thus, the **H₂Vd** ligand platform offers a plethora of interesting outcomes.

2. Experimental section

2.1. General information

o-Vanillin, diethylenetriamine and HEPES buffer were purchased from Sigma-Aldrich. $Zn(NO_3)_2 \cdot 6H_2O$, $ZnBr_2$, ZnI_2, $Cd(NO_3)_2 \cdot 4H_2O$, and other reagents were procured from LOBA and Merck India, respectively. The buffer was prepared using triple distilled water. The solvents used for the spectroscopic studies and for the syntheses were purchased from commercial sources and used as received. Powder X-ray diffraction (PXRD) patterns were acquired using a PANalytical, XPERT-PRO diffractometer (Netherlands) operated at 40 kV, 30 mA, with graphite monochromatized Mo-Kα radiation of wavelength = 0.71073 Å and a nickel filter. Elemental analyses for C, H and N were performed on a PerkinElmer 2400 II analyzer. The FT-IR spectra were recorded from KBr pellets in the range of 400–4000 cm^{-1} on a PerkinElmer Spectrum 100 spectrometer. ^{1}H and ^{13}C-NMR spectra were recorded in d₆-DMSO with TMS as the internal standard on a Bruker, AV 300 Supercon Digital NMR system. The ESI-MS spectra were recorded on a QTof Micro YA263 mass spectrometer. A Systronics digital pH meter (model 335) was used to measure the pH of the solution and the adjustment of pH was done using either 50 mM HCl or NaOH solution. The absorption and emission spectra were recorded on a Hitachi UV-Vis U-3501 spectrophotometer and a PerkinElmer LS55 fluorimeter, respectively. Time-resolved fluorescence lifetime measurements were performed on a Horiba Jobin Yvon Fluorocube 01-NL time-correlated single photon counting (TCSPC) set up by employing a picosecond delta diode (DD-375L) operating at λ_{ex} = 375 nm and a repetition rate of 1 MHz as the excitation source. The overall temporal

and spectral resolutions of the instrument were ~60 ps. The average fluorescence lifetimes (τ_{avg}) were calculated from the decay times and pre-exponential factors using the following equation:

$$\tau_{avg} = \frac{\sum \alpha_i \tau_i^2}{\sum \alpha_i \tau_i}$$

where α_i is the pre-exponential factor corresponding to the ith decay time constant τ_i.

The quantum yield was calculated using the following equation:

$$\phi_s = \phi_R \frac{A_S}{A_R} \times \frac{Abs_R}{Abs_S} \times \frac{\eta_S^2}{\eta_R^2}$$

where the *A* terms denote the integrated area under the fluorescence curve, Abs denotes absorbance, η is the refractive index of the medium and Φ is the fluorescence quantum yield. Subscripts *S* and *R* denote the respective parameters for the studied sample and reference, respectively.

2.2. Theoretical methods

The geometries of the PPi complexes with complex **1a** were fully optimized using the M06-2X/6-31G* level of theory by means of the Gaussian09 software.[19] The M06-2X[20] functional intrinsically includes Grimme's dispersion correction.[21] This functional is adequate for computing transition metal complexes. We have also included solvent effects (water) in the calculations using the polarization continuum model (PCM)[22] as implemented in the Gaussian-09 program.[19]

2.3. Synthesis and characterisation

Synthesis of the ligand (H₂Vd). The Schiff base ligand **H₂Vd** was prepared according to a reported procedure.[23] *o*-Vanillin (0.304 g, 2.0 mmol) was dissolved in ethanol (15 mL). To this, a solution of diethylenetriamine (0.103 g, 1.0 mmol), also dissolved in the same solvent (15 mL), was added dropwise at room temperature. The reaction mixture was then heated under reflux for 5 h and allowed to cool at room temperature. Removal of the solvent in a rota-evaporator afforded **H₂Vd** as a yellow liquid product which was dried overnight under vacuum. Yield: 97%. Anal. calcd for $C_{20}H_{25}N_3O_4$ (371.43): C, 64.67; H, 6.78; N, 11.31; found: C, 64.66; H, 6.79; N, 11.30; ^{1}H-NMR (300 MHz, d₆-DMSO) δ_H: 8.37 (s, 1H, CH=N), 3.65 (s, 3H, OCH₃), 6.62 (t, 1H, Ar), 6.86 (d, 2H, Ar) (Fig. S1†). FT-IR (KBr, cm^{-1}), $\nu_{(O-H)}$ = 3305 cm^{-1}, $\nu_{(C=N)}$ = 1644.86 cm^{-1} (Fig. S5†). ESI-MS *m/z*, ion: 372.19, [**H₂Vd** + H]$^+$ (Fig. S6†).

General procedure for the synthesis of complexes 1(a–c)–2. The four metal complexes have been synthesized using the following general procedure:

H₂Vd (0.371 g, 1.0 mmol) was dissolved in methanol (10 mL). MX₂·nH₂O (M = Zn, X = NO₃, n = 6; M = Zn, X = Br, n = 0; M = Zn, X = I, n = 0; M = Cd, X = NO₃, n = 4) and triethylamine (0.138 mL, 1.0 mmol) were added to this solution. The reaction mixture was refluxed for 4 h to afford a clear solution and then the solution was filtered off. The filtrate was kept

aside undisturbed for slow evaporation. After about two days, single crystals, suitable for X-ray diffraction analysis, were isolated. Specific details of each reaction and the characterization data for these complexes are given below.

[Zn$_2$(Vd·H)$_2$(NO$_3$)$_2$]·CH$_3$OH (1a). Quantities: **H$_2$Vd** (0.371 g, 1.0 mmol), Zn(NO$_3$)$_2$·6H$_2$O (0.594 g, 2.0 mmol), Et$_3$N (0.138 mL, 1.0 mmol). Yield: 81%. Anal. calcd for C$_{40.5}$H$_{50}$N$_8$O$_{14.5}$Zn$_2$ (1011.62): C, 48.08; H, 4.98; N, 11.08; found: C, 48.09; H, 4.99; N, 11.07. FT-IR (KBr, cm^{-1}): $\nu_{(OH)}$ = 3434.14 cm^{-1}, $\nu_{(C=N)}$ = 1634.72 cm^{-1}, $\nu_{(NO_3)}$ = 1468.34 cm^{-1} (Fig. S5†). ESI-MS m/z, ion: 434.11, [(Vd)$_2$ + (Zn)$_2$ + 2H]$^{2+}$ (Fig. S6†).

Zn$_2$(Vd·H)$_2$(Br)$_2$ (1b). Quantities: **H$_2$Vd** (0.371 g, 1.0 mmol), ZnBr$_2$ (0.450 g, 2.0 mmol), Et$_3$N (0.138 mL, 1.0 mmol). Yield: 80%. Anal. calcd for C$_{40}$H$_{48}$Br$_2$N$_6$O$_8$Zn$_2$ (1031.42): C, 46.58; H, 4.69; N, 8.15; found: C, 46.57; H, 4.68; N, 8.16. FT-IR (KBr, cm^{-1}): $\nu_{(OH)}$ = 3305.66 cm^{-1}, $\nu_{(C=N)}$ = 1641.27 cm^{-1} (Fig. S5†). ESI-MS m/z, ion: 434.11, [(Vd)$_2$ + (Zn)$_2$ + 2H]$^{2+}$ (Fig. S6†).

Zn$_2$(Vd·H)$_2$(I)$_2$ (1c). Quantities: **H$_2$Vd** (0.371 g, 1.0 mmol), **ZnI** (0.638 g, 2.0 mmol), Et$_3$N (0.138 mL, 1.0 mmol). Yield: 81%. Anal. calcd for C$_{40}$H$_{48}$I$_2$N$_6$O$_8$Zn$_2$ (1125.38): C, 42.69; H, 4.30; N, 7.47; found: C, 42.68; H, 4.29; N, 7.46. FT-IR (KBr, cm^{-1}): $\nu_{(OH)}$ = 3434.30 cm^{-1}, $\nu_{(C=N)}$ = 1626.97 cm^{-1} (Fig. S5†). ESI-MS m/z, ion: 434.10, [(Vd)$_2$ + (Zn)$_2$ + 2H]$^{2+}$ (Fig. S6†).

Cd$_3$(Vd)$_2$(NO$_3$)$_2$ (2). Quantities: **H$_2$Vd** (0.371 g, 1.0 mmol), Cd(NO$_3$)$_2$·4H$_2$O (0.617 g, 2.0 mmol), Et$_3$N (0.138 mL, 1.0 mmol). Yield: 79%. Anal. calcd for C$_{40}$H$_{46}$Cd$_3$N$_8$O$_{14}$ (1200.05): C, 40.03; H, 3.86; N, 9.34; found: C, 40.02; H, 3.87; N, 9.33. FT-IR (KBr, cm^{-1}) $\nu_{(OH)}$ = 3434.13 cm^{-1}, $\nu_{(C=N)}$ = 1634.46 cm^{-1}, $\nu_{(NO_3)}$ = 1470.66 cm^{-1} (Fig. S5†). ESI-MS m/z, ion: 538.03, [(Vd)$_2$ + (Cd)$_3$ + 2H]$^{2+}$, 965.17, [(Vd)$_2$ + (Cd)$_2$ + H]$^+$ (Fig. S6†).

Synthesis of the PPi complex (3). The PPi complex was synthesized by adding a 5.0 mL aqueous solution of PPi (0.446 g, 1.0 mmol) slowly (over a time period of 0.5 h) to a magnetically stirred 10.0 mL aqueous methanolic solution of complex **1a** (0.506 g, 0.5 mmol). The mixture was further stirred at room temperature for approximately 3.0 h; the solution was filtered and left in open air. After several days a yellow crystalline product was found. Yield: 72%. Anal. calcd for C$_{40}$H$_{50}$N$_6$O$_{15}$Zn$_2$P$_2$ (1044.14): C, 45.86; H, 4.81; N, 8.02; found: C, 45.85; H, 4.80; N, 8.03. FT-IR (KBr, cm^{-1}): $\nu_{(OH)}$ = 3432.79 cm^{-1}, $\nu_{(C=N)}$ = 1635.01 cm^{-1}, $\nu_{(P-O)}$ = 1112.46 cm^{-1} (Fig. S5†). ESI-MS m/z ion: 1085.4316, [(Vd)$_2$ + (Zn)$_2$ + 2P + Na + H$_2$O + 2H]$^+$, C$_{40}$H$_{52}$N$_6$O$_{16}$Zn$_2$P$_2$Na (Fig. S6†).

2.4. Cell study of H$_2$Vd

Materials and methods. The frozen human colorectal carcinoma cell line HCT 116 and HeLa cells were obtained from NCCS, Pune, India and maintained in Dulbecco's modified Eagle's medium (DMEM, Sigma Chemical Co., St Louis, MO, USA) supplemented with 10% fetal bovine serum (Invitrogen), penicillin (100 µg mL^{-1}), and streptomycin (100 µg mL^{-1}). Cells were initially propagated in a 25 cm^2 tissue culture flask under an atmosphere of 5% CO$_2$ and 95% air at 37 °C in a humidified air till 70–80% confluency.

Fluorescence imaging studies. For fluorescence imaging studies, HCT 116 (1 × 10^{-5}) cells in 150 µl medium were seeded on a sterile 12 mm diameter poly-L-lysine coated coverslip and kept in a sterile 35 mm covered petri dish and incubated at 37 °C in a CO$_2$ incubator for 24–30 h. The next day, cells were washed three times with phosphate buffered saline (pH 7.4), fixed using 4% paraformaldehyde in PBS (pH 7.4) for 10 minutes at room temperature, and washed with PBS followed by permeabilization using 0.1% saponin for 10 minutes. Then, the cells were incubated with 2.0 × 10^{-4} (M) Zn(NO$_3$)$_2$·6H$_2$O dissolved in 100 µl DMEM at 37 °C for 1 h in a CO$_2$ incubator and observed under an epifluorescence microscope (Carl Zeiss). The cells were again washed thrice with PBS (pH 7.4) to remove any free metal and incubated in DMEM containing **H$_2$Vd** to a final concentration of 1 × 10^{-6} M followed by washing three times with PBS (pH 7.4) to remove the excess probe outside the cells. Again, images were taken using an epifluorescence microscope. In a separate coverslip undergoing the same treatment the cells were treated with **H$_2$Vd** alone without any zinc salt. Before fluorescence imaging, all the solutions were aspirated out and mounted on slides in a mounting medium containing DAPI (1 µg ml^{-1}) and stored in the dark before microscopic images were acquired.

Cytotoxicity assay. The cytotoxic effects of **H$_2$Vd**, Zn(NO$_3$)$_2$·6H$_2$O and **H$_2$Vd**-Zn^{2+} complexes were determined by an MTT assay following the manufacturer's instructions (MTT 2003, Sigma-Aldrich, MO). HCT cells were cultured in 96-well plates (approximately 10^4 cells per well) for 24 h. The next day, the medium was removed and various concentrations of **H$_2$Vd**, Zn(NO$_3$)$_2$·6H$_2$O and **H$_2$Vd**-Zn^{2+} complexes (0, 20, 30, 50, 75, and 100 µM) were added to the cells and incubated for 24 h. Control samples with no cells and cells in DMEM without any treatment were also included in the study. Following incubation, the growth medium was removed, and fresh DMEM containing MTT solution was added. The plates were incubated for 3–4 h at 37 °C. Subsequently, the supernatant was removed, the insoluble colored formazan product was solubilized in DMSO, and its absorbance was measured on a microtiter plate reader (PerkinElmer) at 570 nm. The assay was performed in triplicate for each concentration of **H$_2$Vd**, Zn(NO$_3$)$_2$·6H$_2$O and **H$_2$Vd**-Zn^{2+} complexes. The OD value of wells containing only DMEM was subtracted from all readings to get rid of the background influence. Data analysis and calculations of standard deviation were performed using Microsoft Excel 2007 (Microsoft Corporation).

2.5. Cell study of complex 1a

Cell lines and chemicals. HCT 116 (Human colorectal carcinoma), HepG2 (human hepatocellular carcinoma) and A549 (human small lung carcinoma) cell lines were purchased from the NCCS, Pune, India. Dulbecco's Modified Eagle's Medium (DMEM), penicillin–streptomycin–neomycin (PSN) antibiotic, fetal bovine serum (FBS), trypsin and ethylenediaminetetraacetic acid (EDTA) were purchased from Gibco BRL (Grand Island, NY, USA). Tissue culture plastic ware was obtained from Nunc (Roskilde, Denmark). 3-(4,5-Dimethylthiazol-2-yl)-2,5-diphenyl-

tetrazolium bromide (MTT) and DAPI (4′,6-diamidino-2-phenyl-indole dihydrochloride) were purchased from SRL (India) and Invitrogen (California), respectively. All other chemicals used were from Sigma Chemical Co. (St Louis, MO, USA).

Cell culture. HCT 116, HepG2 and A549 cells were cultured in DMEM with 10% fetal bovine serum (FBS) and 1% anti-biotic (PSN) at 37 °C in a humidified atmosphere under 5% CO_2. After 75–80% confluency, cells were gathered with 0.25% trypsin and 0.52 mM EDTA in phosphate buffered saline (PBS), and seeded at the required density to allow them to re-equili-brate for a day before starting the experiment.

Cell viability. To determine the cell viability, an MTT [(4,5-di-methylthiazol-2-yl)-2,5-diphenyltetrazolium bromide] assay was performed. For the initial screening, HCT 116, HepG2 and A549 cells were seeded (4×10^3 cells per well) in 96 well plates and kept at 37 °C in a humidified 5% CO_2 atmosphere. Cell viability was examined by treatment of complex **1a** with different concentrations (2, 5, 8, 10 μM). After treatment, plates were kept in an incubator for 24 h. After 24 h of incu-bation, cells were rinsed with PBS and then a MTT solution (4 mg ml^{-1} in PBS) was added into each well and kept in an incubator for 4 h. The absorbance of the solubilised intracellu-lar formazan was calculated at 595 nm using an ELISA reader (model: Emax, Molecular Devices, USA).[24]

Fluorescence microscopy. To observe nuclear damage, cells were treated with complex **1a** at 8 μM and untreated cells were washed with PBS and fixed with 3.7% paraformaldehyde at room temperature for 2 h. Fixed cells were stained with 10 μg ml^{-1} of DAPI (4′,6-diamidino-2-phenylindole dihydrochloride) and observed under a fluorescence microscope with excitation at 359 nm and emission at 461 nm.[25] Cells were analysed under a fluorescence microscope (model: OLYMPUS IX70, Olympus Optical Co. Ltd, Shibuya-ku, Tokyo, Japan). Images were acquired.

Quantification of apoptosis using Annexin-V. Apoptosis was assayed by the use of an Annexin-V FITC apoptosis detection kit (Calbiochem, CA, USA). After treatment of complex **1a** (8 μM) for several hours (0 and 24 h), cells were washed and stained with PI and Annexin-V-FITC in accordance with the manufacturer's instructions. The percentages of live, apoptotic and necrotic cells were evaluated by flow cytometry (BD LSRFortessa™, San Jose, CA, USA). For data of each sample 10^6 cells were analyzed.[26]

2.6. Single-crystal X-ray crystallography

Crystal data were collected for all four crystals with Mo-Kα radi-ation at 150 K using an Oxford Diffraction XCalibur CCD system. Crystals were positioned at 50 mm from the CCD and 321 frames were measured with counting times of 10 s. Data analysis was carried out using the CrysAlis program.[27] The structures were solved by direct methods using the Shelxl-2016-6 program.[28] The non-hydrogen atoms were refined using anisotropic thermal parameters. The hydrogen atoms bonded to carbon and nitrogen were included at geometric positions and given thermal parameters equivalent to 1.2 times those of the atom to which they were attached. Absorption corrections

were carried out using the ABSPACK program.[29] The structures were refined on F^2 using Shelxl-2016-6.[28] The crystallographic data for complexes **1(a–c)** and **2** are summarized in Table S2.† The structure of **1a** contains a solvent methanol molecule which was refined with 50% occupancy. Selected bond para-meters of complexes **1(a–c)** and **2** are given in Table S3.† The crystallographic figures have been generated using Diamond 3.0 software. CCDC no. 1541737, 1541738, 1541742 and 1541744 for **1a**, **1b**, **1c** and **2**, respectively,† contain supplemen-tary crystallographic data for this paper.

3. Results and discussion

3.1. Syntheses and general characterization

The receptor **H₂Vd** was synthesized *via* a one-step simple con-densation reaction in a methanol solution (Scheme 1). The structure was confirmed by ^1H and ^{13}C-NMR spectroscopy, FT-IR spectroscopy, CHN analysis, and ESI-MS spectrometry (Fig. S1, S5 and S6†). The experimental powder XRD patterns of the bulk crystalline material are in good agreement with the simulated XRD patterns of single crystal X-ray diffraction, con-firming the purity of the bulk samples (Fig. S7†).

H₂Vd is a symmetrical ligand bearing two sets of N_{imine}, $O_{phenoxo}$, and $O_{methoxy}$ atoms with a single N_{amine} atom in the middle (Scheme 2). Thus **H₂Vd** is not only a potential bridging ligand but also a very good chelating ligand with as many as eight binding sites (Scheme S2†).[30] In the course of exploring this ligand system, we found that the reaction of **H₂Vd** and $M(NO_3)_2 \cdot nH_2O$ [M = Zn, $n = 6$, M = Cd, $n = 4$] in a 1 : 2 ratio led to the dinuclear zinc complex $[Zn_2(Vd \cdot H)_2(NO_3)_2] \cdot CH_3OH$ (**1a**) and the trinuclear cadmium complex $[Cd_3(Vd)_2(NO_3)_2]$ (**2**). The halide complexes $[Zn_2(Vd \cdot H)_2(Br)_2]$ (**1b**) and $[Zn_2(Vd \cdot H)_2(I)_2]$ (**1c**)] were prepared in a similar manner and were obtained in good yields (80–81%). The bromide complex was bright yellow whereas the iodide complex was orange. In other words, we obtained three dinuclear Zn^{2+} complexes, **1(a–c)**, with $Zn(NO_3)_2$, $ZnBr_2$ and ZnI_2 and a trinuclear Cd^{2+} complex with $Cd(NO_3)_2$(**2**). The chloro complex could not be isolated despite repeated attempts. All the complexes are thermally very stable. In **1(a–c)**, **H₂Vd** exhibits chelating and bridging modes using the η^1: η^1: η^1: η^1: μ_2 (Mode I in Scheme 2) coordination mode. In the case of **2**, each **H₂Vd** employs the η^1: η^2: η^1: η^1: η^1: η^2: η^1: μ_2 (Mode II in Scheme 2) coordination mode. In the FT-IR spectra of the synthesized complexes, the strong bands that appeared around 1626.97–1641.27 cm^{-1} could be ascribed to the stretching vibrations of C=N. **H₂Vd** exhibits an ability to sense Zn^{2+} while the ensemble could be successfully utilized to sense PPi. All the complexes reported here were crystallogra-phically characterized and the molecular structures of **1a**, **1b** and **2** are depicted in Fig. 1, 2 and 3.

3.2. Structure description of $[Zn_2(Vd \cdot H)_2(NO_3)_2] \cdot CH_3OH$ (1a)

Complex **1a** crystallizes in the monoclinic crystal system with space group $P2_1/c$ and features a dimeric Zn(II) moiety. The dimer contains two independent five-coordinate Zn(II) centers
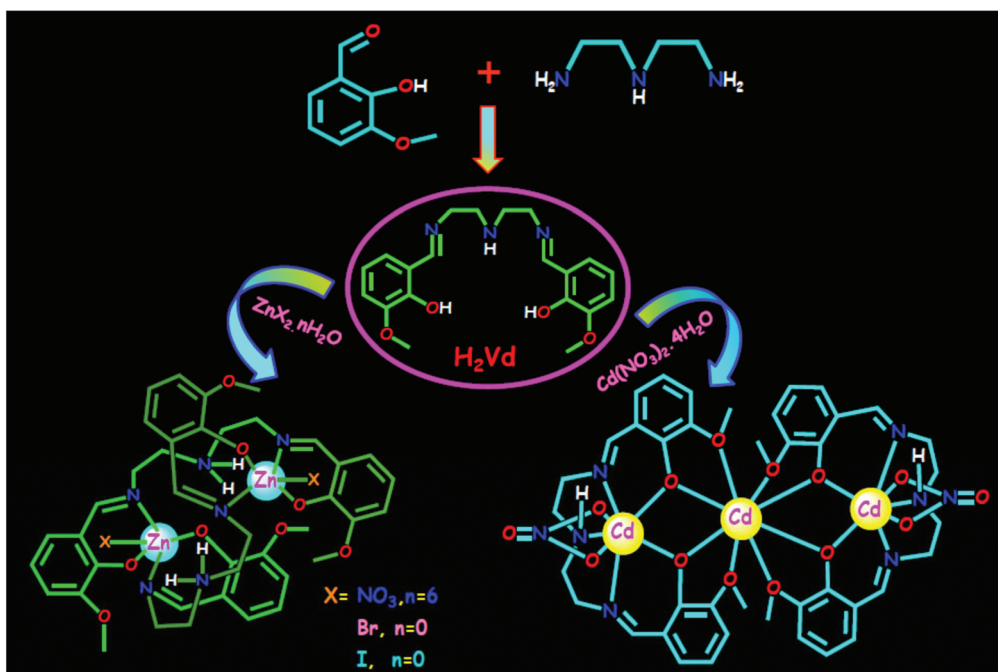
Scheme 1 Synthetic scheme for the synthesis of the ligand (H₂Vd) in complexes **1(a−c)** and **2**.
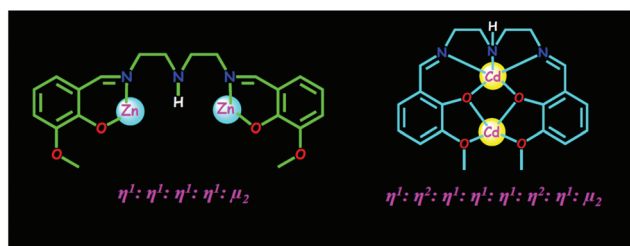
Scheme 2 Coordination and bridging modes of the ligand (H₂Vd) in complexes **1(a−c)** and **2**.

connected by two single protonated **Vd**$^{2-}$ ligands and two co-ordinated nitrito anions to form a $[Zn_2(Vd\cdot H)_2(NO_3)_2]$ dimer. **H₂Vd** binds by means of N_{imine} and $O_{phenoxo}$ whereas $O_{methoxy}$ and N_{amine} remain uncoordinated (Mode I). Thus, each Zn(II) center is coordinated to two sets of N_{imine} and $O_{phenoxo}$ groups from two **H₂Vd** ligands in the equatorial plane with Zn–N_{imine} 2.071(4)–2.081(3) Å, Zn–$O_{phenoxo}$ 1.986(3)–2.009(3) Å, and one oxygen atom from a coordinated nitrito group at distances of 2.267(3) and 2.196(3) Å. The geometries of the coordination spheres are best considered to be distorted trigonal bipyramids with τ values of 0.58 and 0.72, respectively. In this geometry the two nitrogen atoms occupy axial positions at N–Zn–N angles of 175.98(13)° and 177.14(14)° for Zn(1) and Zn(2), respectively. The uncoordinated N_{amine} is protonated, thereby balancing the charge of the complex. The Zn(II) centers lie far apart at a distance of 4.372(1) Å. In addition, one co-crystallized solvent methanol molecule was also found in the X-ray structure with 50% occupancy (Fig. 1). The nitrate ligand
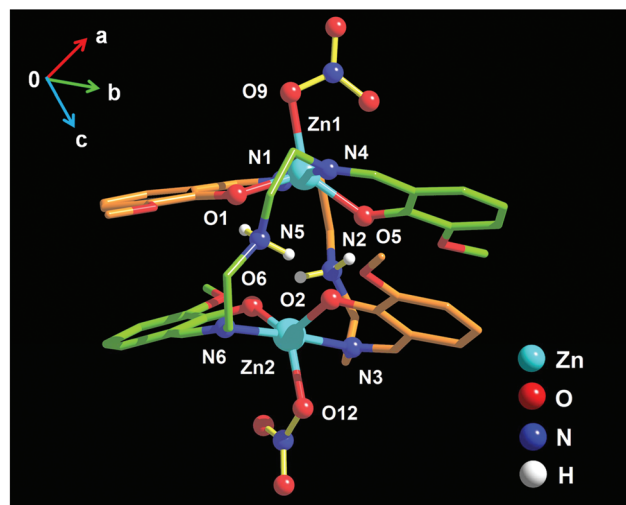

Fig. 1 Solid state structure of complex **1a** with a partial atom numbering scheme (solvent molecule and hydrogen atoms, except those present on N2 and N5, are omitted for clarity).

offers anisobidentate binding mode in **1a** as is evident from the bond length data 2.267(3) and 2.630(4) Å for Zn(1) and 2.196(3) and 2.638(4) Å for Zn(2), as is consistent with the criteria introduced by Kleywegt *et al.*[31] (Table S5†). Therefore, we have performed a Continuous Shape Measurement Analysis considering both five and six coordinated zinc centers and the outcome indicates a five coordinated distorted trigonal bipyramidal geometry with the minimum deviation of 1.385 for Zn(1) and 2.413 for Zn(2) (out of the range 0.1–3, CShM value)
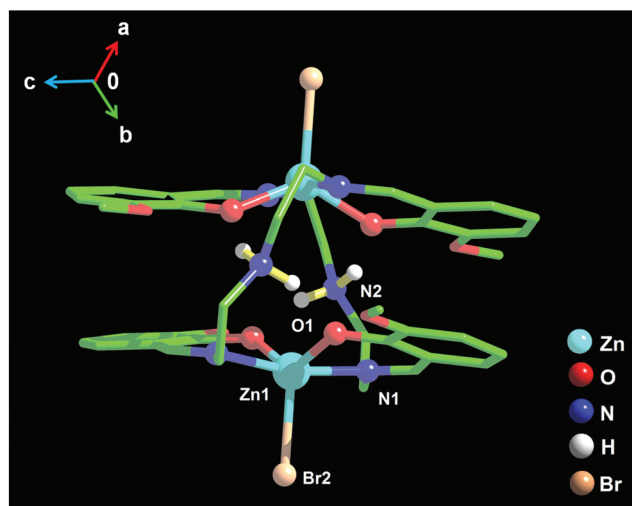
Fig. 2 Solid state structure of complex **1b** with a partial atom numbering scheme. Complex **1c** is isostructural.
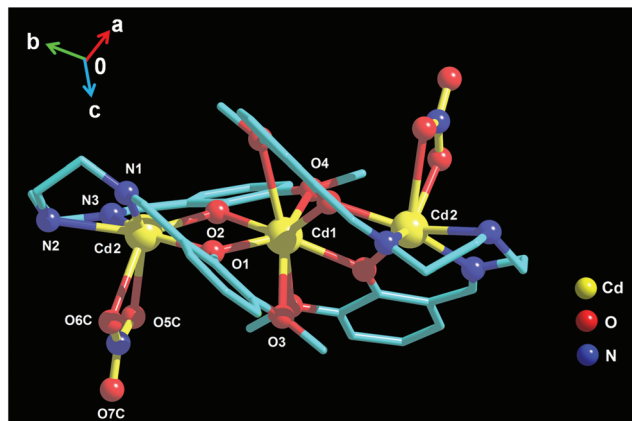

Fig. 3 Solid state structure of complex **2** with a partial atom numbering scheme.

from the ideal D_{3h} symmetry (Table S4†).[32] The two protonated uncoordinated nitrogen atoms N(2) and N(5) at the centre of the ligand form intramolecular hydrogen bonds as listed in Table S6.† It will be noticed that all these amino hydrogen atoms participate as bifurcated donor hydrogen bonds to oxygen atoms, though in each case, one bond is significantly stronger than the other (Fig. S8†). Despite the presence of ligand π-systems in the cations of complex **1a**, there are strong intramolecular π···π (within Cg(7)···Cg(10) = 3.619(3) Å, Cg(8)···Cg(9) = 3.508(3) Å) and intermolecular C–H···π ([C(11)–H(11A)···Cg(9)] = 2.75 Å) interactions between the closest neighbours (Fig. S8†). These few noncovalent π-stacking interactions can be viewed as medium to strong as they exhibit rather short centroid–centroid distances (<3.8 Å) together with small slip angles (β, γ < 25°) and vertical displacements (a < 1.5 Å) between the ring centroids which translate into a sizable overlap of the aromatic planes and are indicative of strong

π-stacking interactions.[33] With respect to C–H···π interactions, in complex **1a**, a single C–H···π contact is found with H···Cg < 3.0 Å and γ < 30° (Scheme S1, Table S7†) which is slightly longer than expected for a medium to strong contact. The dimers form 1D chains through C–H···π interactions (Fig. S8†).

3.3. Structure description of [Zn₂(Vd·H)₂(Br)₂] (1b) and [Zn₂(Vd·H)₂(I)₂] (1c)

Single crystal X-ray diffraction structural analysis reveals that **1b** and **1c** are isomorphous, crystallizing in the tetragonal space group $I4_1/acd$ and feature a dimeric unit, $Zn_2(Vd·H)_2(X)_2$ (where X = Br for **1b**, I for **1c**), which contains two C_2 axes, one through the Zn_2X_2 unit and the other through the two N2 atoms as shown in Fig. 2. Each Zn(II) is five coordinated with the coordination sites occupied by two N_{imine} (Zn–N_{imine} = 2.135(3), 2.135(3) Å for **1b** and **1c**, respectively), two $O_{phenoxo}$ (Zn–$O_{phenoxo}$ = 1.992(2) Å (**1b**)/1.986(3) Å (**1c**)) from two different H_2Vd ligands and one bromine/iodine (Zn–Br/I = 2.459(1)/2.671(1) Å). The dimeric structures in **1b** and **1c** are therefore similar to those found in **1a**, but are constrained by the crystallographic two-fold axes. In the two structures, the environment of the metal atoms is five-coordinate trigonal bipyramidal as indicated by the τ values of 0.64 and 0.67. Continuous Shape Measurement Analysis confirms distorted trigonal bipyramidal geometry for both **1b** and **1c** (Table S4†). Furthermore, the Zn···Zn separations of 4.516(1) and 4.441(1) Å, respectively, are slightly higher than the value found in **1a**. As in the structure of **1a**, the non-bonded nitrogen atoms at the centre of the ligand are protonated and form intramolecular hydrogen bonds to adjacent oxygen atoms (Table S6†). In complexes **1b** and **1c** the intramolecular and intermolecular packing along the crystallographic direction is controlled by π-stacking interactions[33,34] between the aromatic rings. The ring slippage has slip angles of 21.6° (**1b**) and 21.1° (**1c**) and a vertical displacement between the ring centroids of 1.39 Å (**1b**) and 1.38 Å (**1c**) (centroid separation within Cg(3)···Cg(3) = 3.778(3) Å (**1b**)/3.829(3) Å (**1c**)). Therefore, the π-stacking in complexes **1b** and **1c** corresponds closely to strong intramolecular π···π interactions which are described in the above section. In addition, intermolecular C–H···π ([C(10)–H(10A)···Cg(3)] = 2.89 Å (**1b**)/2.91 Å (**1c**)) and van der Waals (C(8)–H(8B)···H(5)–C(5) = 2.34 Å (**1b**)) interactions between neighbouring molecules are also present (Fig. S10†), which assist in the formation of a 3D supramolecular polymeric network within the crystal (as shown in Fig. S9†).

3.4. Structure description of Cd₃(Vd)₂(NO₃)₂(2)

Crystal structure analysis of **2** reveals a 3D framework within the monoclinic $C2/c$ space group. The asymmetric unit contains two crystallographically independent Cd(II) centers that using different coordination geometries, one Vd^{2-} and one coordinated nitrito ligands. As depicted in Fig. 3, the central Cd(1) atom is positioned on a crystallographic two-fold axis and bonded only to oxygen atoms. By contrast, the symmetry equivalent terminal Cd(2) atoms are each bonded to five atoms (O1$_{phenoxy}$, N1$_{imine}$, N2$_{amine}$, N3$_{imine}$, O2$_{phenoxy}$) of a Vd^{2-} ligand

and an additional nitrate anion to form highly distorted seven-co-ordinate environments. The shape of the heptacoordinated Cd(2) (and its symmetry equivalent Cd($2^{#}$)) appears to be far from any reference geometry, which is rather uncommon (Table S4†). Bond lengths in the coordination sphere follow a wide range (Cd(2)–O(1) = 2.236(2) Å, Cd(2)–N(1) = 2.299(3) Å, Cd(2)–N(3) = 2.313(4) Å, Cd(2)–N(2) = 2.523(4) Å, Cd(2)–O(2) = 2.350(2) Å). The nitrate is bonded via O(5C) at 2.347(3) and O(6C) at 2.750(4) Å distances, which, according to the criteria introduced by Kleywegt et al.[31] (Table S5†), demonstrates a nearly anisobidentate binding mode. The two phenoxy oxygen atoms O(1) and O(2) bridge Cd(2) to the central Cd(1) atom at distances of 2.203(2) and 2.287(2) Å. The central Cd(1) atom is also bonded to methoxy oxygen atoms O(3) and O(4) at 2.740(3) and 2.451(3) Å, thus completing a highly distorted eight-coordinate environment which is described from continuous Shape Measurement Analysis (CShM) as having a distorted tri-angular dodecahedron geometry. The linkage between terminal and central Cd(ɪɪ) centers is established by means of $O_{phenoxo}$ groups coming from two **H₂Vd** ligands. Two Cd_2O_2 rhombs thus formed are fused at the middle Cd(ɪɪ) center (Cd1) and the dihedral angle between the planes is 63.0(1)°. The resulting trinuclear species, $Cd_3(\textbf{Vd})_2(NO_3)_2$, contains a nearly linear chain (Cd–Cd–Cd = 155.68(1)°). The Cd(1)···Cd(2) separation is 3.6745(3) Å and the Cd(2)···Cd(2) distance is 7.184(1) Å. The crystal structure of complex **2** reveals the presence of strong intramolecular face-to-face slipped π···π stacking interactions between two aromatic rings with a centroid to centroid distance of 3.697(3) Å (within Cg(1)···Cg(1)), a slip angle of 21.0°, a normal distance of 3.450 Å, and a vertical displacement of 1.33 Å. In addition, the intermolecular hydrogen bonds C(9)–H(9A)···O(5C) and C(12)–H(12)···O(6C) with distances of 3.171(6) and 3.305(6) Å, respectively, shown in Table S6† and van der Waals (C(19)–H(19B)···H(11B)–C(11) = 2.34 Å) interactions produce a supramolecular polymeric association within 2D sheets. The trinuclear units in complex **2** are self-assembled through intermolecular C–H···π [with C(19)–H(19C)···Cg(1) = 2.73 Å] interactions, resulting in the generation of a three-dimensional network, which, in turn, may be considered to be the interlinking of two-dimensional sheets propagated along the crystallographic b axis (Fig. S11†).

3.5. Photophysical properties of H₂Vd in the presence of Zn²⁺

UV-Vis spectra recorded for **H₂Vd** in HEPES buffer (pH = 7.4) solution indicated an absorption maximum at 420 nm, which may have originated from an intra-molecular π–π* charge transfer (CT) transition. Upon addition of Zn²⁺, the intensity of the 420 nm band of **H₂Vd** decreased with the concomitant appearance of a new band at 360 nm (Fig. S12†). A Job's plot at 360 nm indicated a 1:1 stoichiometry of the complex formed between **H₂Vd** and Zn²⁺ (Fig. S13†) and the binding constant (K), determined using the Benesi–Hildebrand expression, was found to be 34.362×10^4 M⁻¹ (Fig. S14†).

The fluorescence titration of **H₂Vd** towards representative metal ions, like Li⁺, Na⁺, K⁺, Ca²⁺, Mg²⁺, Mn²⁺, Ba²⁺, Cu²⁺, Fe²⁺, Cd²⁺, Hg²⁺, Ni²⁺, Pb²⁺, Sr²⁺, Co²⁺, Al³⁺, Cr³⁺, and its selectivity

for Zn²⁺ in HEPES buffer (pH = 7.4) solution were further investigated (Fig. 4). As shown in Fig. 4, **H₂Vd** displayed weak emission (Φ = 0.024) at 467 nm (λ_{ex} = 360 nm). Upon the addition of various concentrations of Zn²⁺, a prompt change of the emission intensity of **H₂Vd** was observed, leading to a 19-fold enhancement of the emission maxima at 467 nm (Φ = 0.454). The observed fluorescence enhancement is a direct consequence of the formation of a rigid system after binding of **H₂Vd** with Zn²⁺, causing the chelation enhanced fluorescence effect (CHEF) to become operative.[35] Additionally, intramolecular hydrogen bonds are formed between phenolic OH and amine nitrogen, which is responsible for excited state intramolecular proton transfer (ESIPT).[35] As already mentioned in the structural description, the probe-Zn²⁺ ensemble is generated as a result of deprotonation of the phenolic OH group inhibiting ESIPT, thereby rationalizing fluorescence
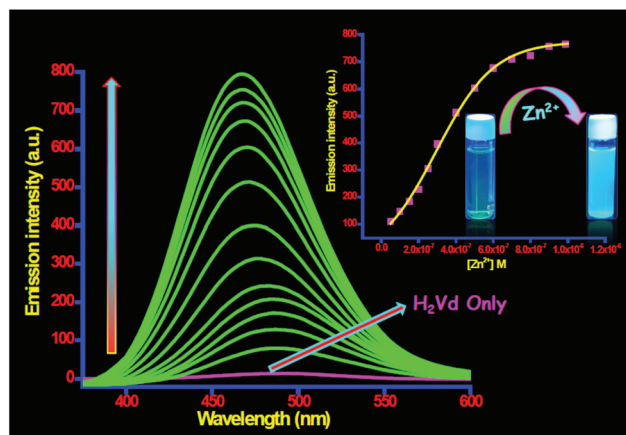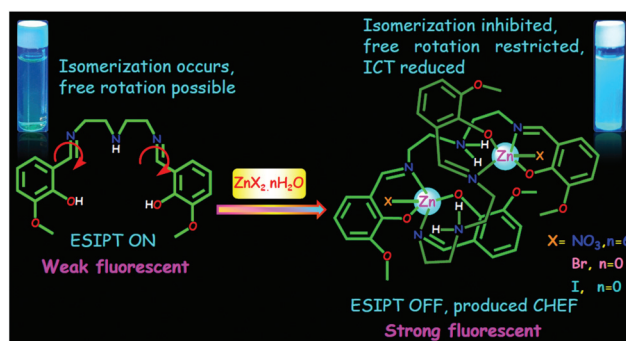

Fig. 4 Emission spectra of **H₂Vd** (5 × 10⁻⁷ M) in the presence of increasing amounts of [Zn²⁺] (0, 0.5, 1, 1.5, 2, 2.5, 3, 4, 5, 6, 7, 8, 9 and 10 (×10⁻⁷) M) in HEPES buffer (pH = 7.4) solution (λ_{ex} = 360 nm, λ_{em} = 467 nm). Inset: Fluorescence emission intensity of **H₂Vd** at 467 nm as a function of [Zn²⁺] and the visual color change observed with the addition of Zn²⁺ ions to **H₂Vd** solution as seen under UV light (λ = 365 nm).

Scheme 3 Schematic illustration of the proposed mechanism for the fluorescence changes of the chemosensor (**H₂Vd**) upon the addition of Zn²⁺.

enhancement (Scheme 3). The Benesi–Hildebrand expression supports a 1:1 stoichiometry between Zn^{2+} and **H₂Vd** having an association constant of 31.647×10^4 M^{-1} (Fig. S15†). We have calculated the stability constants of the complexes between all other metal ions and the ligand apart from Zn^{2+} to assess the complexation properties of other metal ions (Table S9†). The experimental data reinforce that Zn^{2+} forms the most stable complex with the ligand **H₂Vd**. The detection limit (LOD) for **H₂Vd**-Zn^{2+} was estimated to be 6.72×10^{-9} (M) on the basis of fluorescence titration measurements (Fig. S16†).

To evaluate the selectivity of the probe **H₂Vd** towards Zn^{2+}, competition experiments were performed. As shown in Fig. 5, no significant fluorescence increase was observed at 467 nm upon the addition of 4 equiv. of different metal ions *viz.* Li^+, Na^+, K^+, Ca^{2+}, Mg^{2+}, Mn^{2+}, Ba^{2+}, Cu^{2+}, Fe^{2+}, Cd^{2+}, Hg^{2+}, Ni^{2+}, Pb^{2+}, Sr^{2+}, Co^{2+}, Al^{3+} and Cr^{3+}. In contrast, 2 equiv. of Zn^{2+} significantly enhanced the fluorescence intensity at 467 nm.

To monitor the influence of pH on the fluorescence response, probes **H₂Vd** and Zn^{2+} were mixed in different sets of pH (pH 2.0–12.0). Fig. S17† indicated that the optimum performance was observed in the pH range from 5.0 to 9.0. Hence, pH 7.4 was maintained throughout the Zn^{2+} sensing studies as this value was closer to the physiological pH.

The strong fluorescence turn-on was associated with the formation of a complex between Zn^{2+} and the probe moiety, which suppressed both the PET (photoinduced electron transfer) and ESIPT (excited state intramolecular proton transfer) and induced rigidity in the resulting complex, resulting in CHEF (chelation enhanced fluorescence).

The fluorescence average lifetime of **H₂Vd** was measured in the presence and absence of Zn^{2+} ions in HEPES buffer (pH = 7.4) solution (Fig. S24†) and the results are tabulated in Table S8.† The data also indicate that the fluorescence enhancement due to the increase of the ratio of k_r/k_{nr} is primarily due to the reasonable decrease of k_{nr}, supporting a CHEF effect.
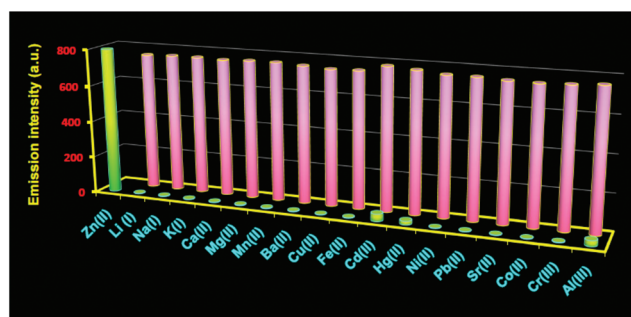
¹H-NMR and ¹³C-NMR titration experiments were used to ascertain the binding mode of **H₂Vd** and Zn^{2+}. NMR spectra of **H₂Vd** were recorded in d_6-DMSO solution and the observed peaks with their chemical shifts (ppm) along with the corresponding assignments are given in Table S1.† Significant spectral changes were observed upon the addition of various concentrations of Zn^{2+} to the solution of **H₂Vd**. In particular, the proton H_a signal experienced a substantial downfield shift at 0.35 ppm as shown in Fig. S2.† On the addition of 2.0 equiv. Zn^{2+} to **H₂Vd** solution, the C_a carbon signal showed a downfield shift of 24.7 ppm. These results indicate coordination of Zn^{2+} with the imine nitrogen atom as expected from single crystal X-ray diffraction studies.

3.6. Response of complex 1a towards PPi

UV-Vis spectral signatures revealed that the peak at 368 nm increases and a new peak appears at 431 nm upon the addition of increasing amounts of PPi to HEPES buffer (pH = 7.4) solution (Fig. S18†). The effect of addition of anionic substrates to the fluorescence spectrum of complex **1a** was examined in HEPES buffer (pH = 7.4) solution (Fig. 6). In the absence of an anionic substrate, the fluorescence spectrum of the receptor complex **1a** (5×10^{-7}) M exhibits a strong emission at 467 nm upon excitation at 360 nm along with a red shift of 11 nm. The addition of 2.0 equiv. of PPi to the solution of complex **1a** induces 16-fold quenching of fluorescence intensity ($\Phi = 0.028$). The fluorescence intensity of complex **1a** exhibits an excellent linear relationship ($R^2 = 0.997$) as a function of the concentration of PPi at 478 nm (Fig. S23†). The limit of detection (LOD) was calculated to be as low as 5.12×10^{-9} (M) (based on DL = $K \times \sigma/S$ where $K = 3$, σ denotes the standard deviation of the blank solution and S denotes the slope of the calibration curve[36] (Fig. S23†)), which is lower

Fig. 5 Fluorescence emission spectra of **H₂Vd** (5×10^{-7} M) in the presence of 4 equiv. of different cations except 2 equiv. of Zn^{2+} in solution [the green bar portion]. Fluorescence intensity of a mixture of **H₂Vd** (5×10^{-7} M) with other metal ions (20×10^{-7} M) followed by the addition of Zn^{2+} (10×10^{-7} M) to the HEPES buffer (pH = 7.4) solution [the red bar portion] ($\lambda_{ex} = 360$ nm, $\lambda_{em} = 467$ nm).

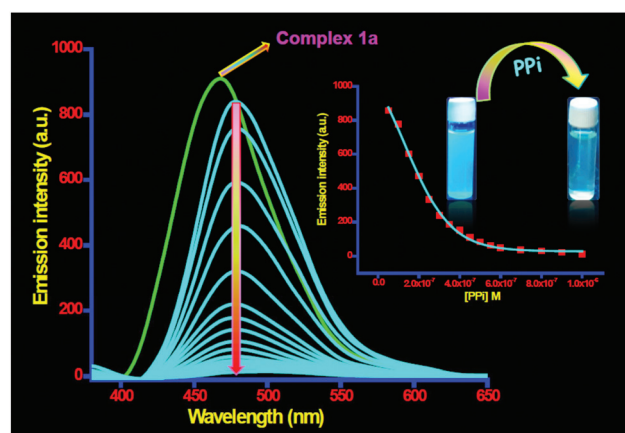**Fig. 6** Emission spectra of complex **1a** (5×10^{-7} M) upon a gradual increase in the concentration of PPi (0, 0.5, 1, 1.5, 2, 2.5, 3, 3.5, 4, 4.5, 5, 5.5, 6, 7, 8, 9 and 10 (×10⁻⁷) M) in HEPES buffer (pH = 7.4) solution ($\lambda_{ex} = 360$ nm, $\lambda_{em} = 478$ nm). Inset: Fluorescence emission intensity changes for the titration of complex **1a** with [PPi] and the visual color change observed with the addition of PPi to complex **1a** solution as seen under UV light ($\lambda = 365$ nm).

than that of many reported PPi chemosensors.[17] In order to prove the selectivity of complex **1a** towards PPi, we carried out fluorescence titration experiments on complex **1a** with other anions (F^-, Cl^-, Br^-, I^-, CH_3COO^-, HCO_3^-, NO_2^-, SO_4^{2-}, PO_4^{3-}, AMP, ADP, and ATP) in HEPES buffer (pH = 7.4) solution. As depicted in Fig. S19,† only PPi provided significant fluorescence-quenching response, which enabled complex **1a** to be sensitive enough for tracing PPi in biosystems. Furthermore, a competitive experiment was performed upon mixing complex **1a** with 4.0 equiv. of different anions and Fig. 7 demonstrates that the fluorescence quenching behaviour of complex **1a** remained more or less unchanged. Complex **1a** presents another interesting feature as it can be used as a colorimetric sensor for PPi. The ability of complex **1a** as a colorimetric probe for PPi was demonstrated using a hand-held camera in the presence of other competing anions (Fig. S20†). Therefore, combining results of its outstanding response behavior, complex **1a** presents robust analytical potential for PPi detection.

Stoichiometry plot (Fig. S21†) analysis of the absorbance titration profile of complex **1a** revealed a 1 : 1 stoichiometry between complex **1a** and PPi species. This was further supported by ESI-MS data (Fig. S6†), which detected a peak at $m/z = 1085.4316$, attributed to $[(Vd)_2 + (Zn)_2 + 2P + Na + H_2O + 2H]^+$, $C_{40}H_{52}N_6O_{16}Zn_2P_2Na$.

The binding affinity of complex **1a** towards PPi at pH 7.4 in HEPES buffer is investigated by using the fluorescence titration experiment and the output is depicted in Fig. S22.† The fluorescence data gave the best fit for a 1 : 1 model of complex **1a** and PPi, and the association constant was estimated to be 13.69×10^5 (M^{-1}) from a Benesi–Hilderbrand plot (Fig. S22†). ESI-MS data of this solution further support the formation of a 1 : 1 complex between PPi and complex **1a**.

Fig. S3† presents an overview of the ^{1}H-NMR spectral output of the result of gradual addition of PPi (0, 0.5, 1.0, 1.5 and 2.0 equiv.) to complex **1a**. The resultant spectrum bears a clear sign of perturbation, indicating definite interaction between complex **1a** and PPi.
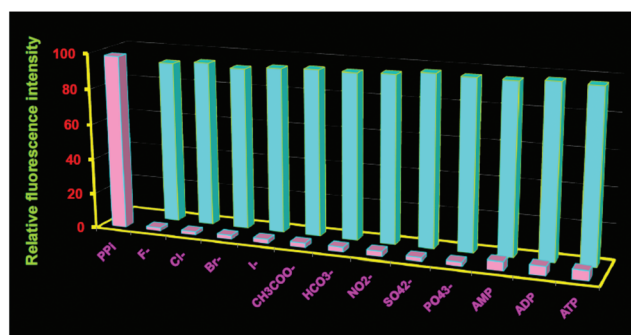
To obtain additional information on the binding mode between PPi and complex **1a**, ^{31}P-NMR spectroscopy studies were undertaken. As shown in Fig. S4,† both P atoms in PPi are magnetically equivalent and appear as a symbolic peak at −5.90 ppm. However, upon binding with complex **1a**, significant downfield shifts of ^{31}P signals ($\Delta\delta$ = 2.75 ppm) were observed. The presence of a single ^{31}P signal suggests that both P atoms in the metal bound PPi are magnetically equivalent and therefore the two sets of oxygen anions on each P atom of PPi are in similar chemical environments and are equally bound to the dinuclear zinc complex.

Lack of conclusive experimental evidence regarding the structure of the PPi–complex **1a** assembly prompted us to perform structure optimization using DFT calculations (M06-2X/6-31G*). From a preliminary conformational search and using several initial geometries for PPi in the geometry optimizations, we have obtained two possible binding modes (two energy minima) for the interaction of PPi with complex **1a**. Since the experimental pH is adjusted at 7.4, we have used the $H_2P_2O_7^{2-}$ ionization form of the PPi anion. The geometries of the two possible binding modes are shown in Fig. 8 along with their relative energies using water as the solvent. In one binding mode (Fig. 8a), one Zn(II) is six-coordinated (two coordination bonds with PPi and four with the organic ligands) and in the other, Zn(II) is five-coordinated (one coordination bond to PPi and four with the organic ligands). In this second binding mode (the most stable thermodynamically), both Zn(II) metal centers are five coordinated (monocoordinated to PPi) and the geometry is similar to a pseudorotaxane where the PPi is acting as the axle. This binding mode (Fig. 8b) is more favorable because the $R_2NH_2^+$ positively charged groups are closer to the anion. Moreover, this binding mode is only achievable for this anion and it is not possible for the rest of the inorganic anions since they are smaller, thus explaining the selectivity. Only ATP could present this binding mode and its lower selectivity is likely due to steric effects. Finally, we have also used other ionization states of the anion ($HP_2O_7^{3-}$ and $P_2O_7^{4-}$) and their binding mode is very similar to that shown in Fig. 8b.

3.7. Construction of the INHIBIT logic gate

The feasibility of applying both the sensing phenomena as a logic gate system was investigated. As shown in Fig. S25,† the fluorescence turn "on" (output "1") happens when Zn^{2+} is the

Fig. 7 Fluorescence Quenching Efficiency (**FQE**), $[\{(F_0 - F)/F_0\} \times 100]$ of complex **1a** (5×10^{-7} M) in the presence of 2.0 equiv. of different anions in solution [the pink bar portion]. Fluorescence Quenching Efficiency (**FQE**) of a mixture of complex **1a** (5×10^{-7} M) with other anions followed by the addition of PPi (10×10^{-7} M) to the HEPES buffer (pH = 7.4) solution [the cyan bar portion].
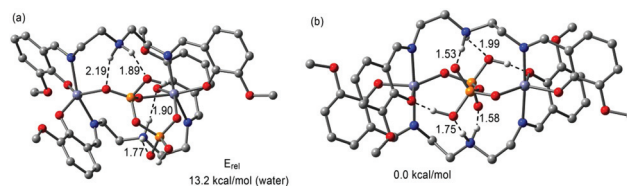

Fig. 8 M06-2x/6-31G* optimized geometries (a, b) of PPi complexes with **1a**. Hydrogen atoms are omitted for clarity, apart from those belonging to the NH_2 groups and the PPi guest. Distances are in Å.

only input. Introduction of PPi into the ensemble H_2Vd-Zn^{2+} leads to turn "off" of the fluorescence response. Thus, output "1" is obtained when the only input is Zn^{2+} and output "0" is obtained when the input is either PPi or both inputs are absent, *viz.*, Zn^{2+} and PPi. It is clear from the truth table that a combination of both inputs leads to fluorescence quenching, resulting in output 0. These results are in accordance with the proper execution of the INHIBIT logic gate.

3.8. Application of H_2Vd for Zn^{2+} detection in live cells

H_2Vd has a thermodynamically favourable binding affinity towards $Zn(NO_3)_2 \cdot 6H_2O$ and both of these form a H_2Vd-Zn^{2+} complex which gives an emission spectrum in the visible range. Keeping this in mind it was conceived that this compound could be exploited for fluorescence imaging of live cells, particularly for sensitive detection of intracellular zinc. However, to materialize this objective it is a prerequisite to assess the cytotoxic effect of H_2Vd, $Zn(NO_3)_2 \cdot 6H_2O$ and the H_2Vd-Zn^{2+} complex on live cells. The well-established MTT assay, which is based on mitochondrial dehydrogenase activity of viable cells, was used to study the cytotoxicity of the above-mentioned compounds at the varying concentrations mentioned in the Experimental section. Fig. S26† shows that H_2Vd did not exert any adverse effect on cell viability at lower concentration, as is also the case when cells were treated with $Zn(NO_3)_2 \cdot 6H_2O$ at lower concentration. However, exposure of HCT cells to the H_2Vd-Zn^{2+} complex resulted in a decline in cell viability above 20 μM concentration. The effect was more pronounced at higher concentration and showed an adverse cytotoxic effect in a dose-dependent manner. The observed cytotoxic effect could be attributed to H_2Vd-Zn^{2+} complex formation. The results obtained in the cytotoxic assay suggested that, in order to pursue fluorescence imaging studies of the H_2Vd-Zn^{2+} complex in live cells, it would be prudent to choose a working concentration of 20 μM for H_2Vd. Hence, to assess the effectiveness of the compound as a H_2Vd for intracellular detection of Zn^{2+} by fluorescence microscopy, HCT cells were treated with 20 μM $Zn(NO_3)_2 \cdot 6H_2O$ for 1 h followed by 10 μM H_2Vd solution to promote the formation of the H_2Vd-Zn^{2+} complex. Fluorescence microscopic studies revealed no fluorescence in cells when treated with either H_2Vd or $Zn(NO_3)_2 \cdot 6H_2O$ alone (Fig. 9a and b). Upon incubation with $Zn(NO_3)_2 \cdot 6H_2O$ followed by H_2Vd, a striking switch-ON fluorescence was observed inside the cells, which indicated the formation of the H_2Vd-Zn^{2+} complex (Fig. 9), as observed earlier in solution studies. Furthermore, an intense blue fluorescence was observed in the cytoplasmic region but not in the nucleus. The fluorescence microscopic analysis strongly suggested that H_2Vd could readily cross the membrane barrier, permeate into HCT cells, and rapidly sense intracellular Zn^{2+}. It is significant to mention here that bright field images of the treated cells did not reveal any gross morphological changes, which suggested that the cells were viable. These findings open up avenues for future *in vivo* biomedical applications of the sensor.
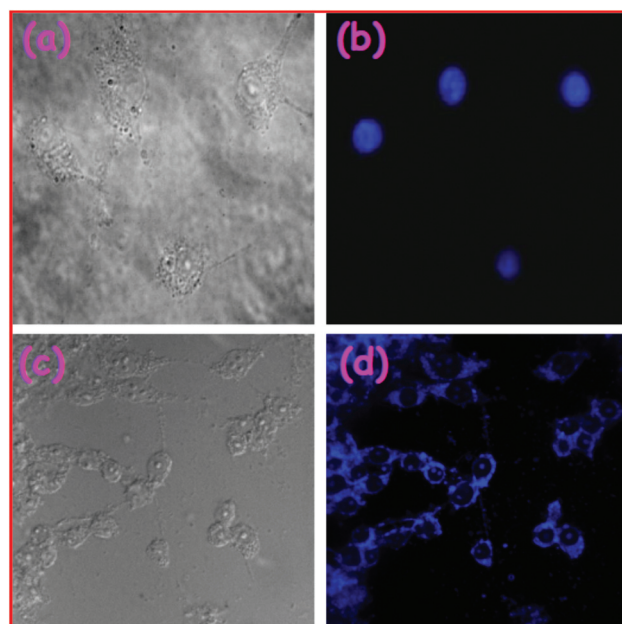

Fig. 9 Fluorescence confocal microscopic images of the probe H_2Vd and $Zn(NO_3)_2 \cdot 6H_2O$ in HCT 116 cells. All images were acquired with a 40× objective lens. (a) Bright field image of the cells without any treatment. (b) Cells treated with only zinc salt (20 μM), nuclei counterstained with DAPI (1 μg mL^{-1}). (c) Bright field image of cells treated with a Zn probe, H_2Vd (20 μM) and $Zn(NO_3)_2 \cdot 6H_2O$ (20 μM). (d) Dark field image of (c), nuclei counterstained with DAPI (1 μg mL^{-1}).

3.9. Anticancer activity of complex 1a

The cytotoxicity of complex **1a** on A549, HepG2 and HCT 116 cells was examined by MTT assay to establish the cellular death response. Treatment with different concentrations of complex **1a** (2, 5, 8 and 10 μM) for 24 h reduced the cell viability significantly in a dose-dependent manner with a lower IC_{50} value of 8.00 ± 1.28 μM for A549 cells (Fig. 10a). Thus, a concentration of 8 μM was chosen for the entire experimentation using A549 cells.

In order to determine whether the cytotoxic effect of complex **1a** was directly connected with apoptosis, morphological analysis of the treated cells was performed using immunofluorescence microscopy as apoptotic cells have some morphological changes like cell shrinkage, rounding, nuclear condensation and DNA fragmentation. The morphological changes of the treated HCT 116 cells were assessed using DAPI staining (nuclear staining dye). The quantity of dense bright fragmented nuclei was markedly increased under complex **1a** treated conditions after DAPI staining when compared with the untreated control (Fig. 10b). To investigate whether complex **1a** was involved in apoptosis/necrosis, flow cytometric evaluation was conducted using Annexin-V-FITC/PI staining by studying the level of exposed phosphatidylserine in the outer membrane of cells. The results showed that the percentage of apoptotic (early and late) cells was increased after 24 h of treatment of complex **1a** (8 μM) (Fig. 10c).
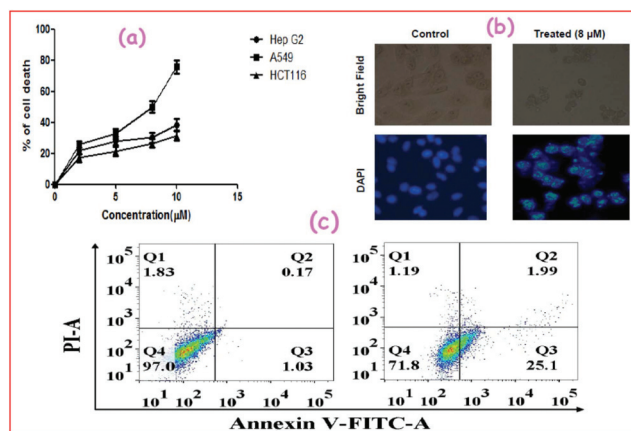
Fig. 10 (a) Effect of increasing doses (0–10 µM) of complex **1a** on different cancer cell lines in 24 h. (b) Morphological and nuclear changes of A549 cells, treated and control: bright field (upper panel) and DAPI (lower panel). (c) Comparative study of Annexin V-FITC/PI positive cells after treatment with 8 µM of complex **1a** by flow cytometry with the control.

4. Conclusions

In summary, we have integrated the structural aspects, sensing behavior and anticancer activity of a flexible ligand, N_1,N_3-bis (3-methoxysalicylidene) diethylenetriamine (**H₂Vd**), and its coordination complexes, to offer a versatile platform. The ligand afforded three dinuclear Zn(II) complexes with Zn (NO₃)₂·6H₂O, ZnBr₂, ZnI₂ and one trinuclear Cd(II) complex with Cd(NO₃)₂·4H₂O. The sensing potential of the ligand was tested by fluorescence spectroscopy and **H₂Vd** offers selective and sensitive detection of Zn(II) in aqueous solution as well as in live HCT 116 cells. Furthermore, the **H₂Vd**-Zn²⁺ complex can successfully sense PPi over other common phosphates in aqueous solution by visual detection as well as fluorimetrically. The proposed structure of the aggregate between the **H₂Vd**-Zn²⁺ complex and PPi was justified using DFT calculations. An INHIBIT logic gate system was established by utilizing the sensing phenomena of Zn²⁺ and PPi. The **H₂Vd**-Zn²⁺ complex also exhibits notable anticancer activity when tested with HCT 116 cells. Together, our experimental outputs highlight that the ligand and its coordination complexes are greatly promising for structural, analytical, bio-medical and bio-electronic applications.

Acknowledgements

Notes and references

1 (*a*) X. Q. Zhang, Y. F. Gao, H. T. Liu and Z. L. Liu, *CrystEngComm*, 2015, **17**, 6037–6043; (*b*) H. Hahm, S. Kim, H. Ha, S. Jung, Y. Kim, M. Yoon and M. Kim, *CrystEngComm*, 2015, **17**, 8418–8422; (*c*) J. He, M. Zeller, A. D. Hunter and Z. Xu, *CrystEngComm*, 2015, **17**, 9254–9263; (*d*) H. L. Nguyen, F. Gandara, H. Furukawa, T. L. Doan, K. E. Cordova and O. M. Yaghi, *J. Am. Chem. Soc.*, 2016, **138**, 4330–4333.

2 (*a*) X. S. Wu, J. Liang, X. L. Hu, X. L. Wang, B. Q. Song, Y. Q. Jiao and Z. M. Su, *Cryst. Growth Des.*, 2015, **15**, 4311–4317; (*b*) B. Mohapatra and S. Verma, *Cryst. Growth Des.*, 2016, **16**, 696–704; (*c*) K. Banerjee, S. Roy, M. Kotal and K. Biradha, *Cryst. Growth Des.*, 2015, **15**, 5604–5613; (*d*) C. Wang, F. Xing, Y. L. Bai, Y. Zhao, M. X. Li and S. Zhu, *Cryst. Growth Des.*, 2016, **16**, 2277–2288; (*e*) D. Singh and C. M. Nagaraja, *Cryst. Growth Des.*, 2015, **15**, 3356–3365; (*f*) X. C. Shan, F. L. Jiang, D. Q. Yuan, M. Y. Wu, S. Q. Zhang and M. C. Hong, *Dalton Trans.*, 2012, **41**, 9411–9416.

3 (*a*) A. B. Nowakowski, J. W. Meeusen, H. Menden and H. Tomasiewicz, *Inorg. Chem.*, 2015, **54**, 11637–11647; (*b*) F. Jones, *CrystEngComm*, 2012, **14**, 8374–8381; (*c*) L. Guang and J. T. Hupp, *J. Am. Chem. Soc.*, 2010, **132**, 7832–7833; (*d*) L. G. Beauvais, M. P. Shores and J. R. Long, *J. Am. Chem. Soc.*, 2000, **122**, 2763–2772.

4 (*a*) M. Andruh, *Chem. Commun.*, 2011, **47**, 3025–3042; (*b*) M. Andruh, *Dalton Trans.*, 2015, **44**, 16633–16653; (*c*) J. Long, F. Habib, P. H. Lin, I. Korobkov, G. Enright, L. Ungur, W. Wernsdorfer, L. F. Chibotaru and M. Murugesu, *J. Am. Chem. Soc.*, 2011, **133**, 5319–5328.

5 (*a*) E. C. Webb, *Enzyme Nomenclature: Recommendations of the Nomenclature Committee of the International Union of Biochemistry and Molecular Biology*, Academic Press, New York, 1992; (*b*) J. Emsley, *Nature's Building Blocks: An A–Z Guide to the Elements*, Oxford University Press, Oxford, 2011.

6 (*a*) A. I. Bush, *Trends Neurosci.*, 2003, **26**, 207–214; (*b*) D. Noy, I. Solomonov, O. Sinkevich, T. Arad, K. Kjaer and I. Sagi, *J. Am. Chem. Soc.*, 2008, **130**, 1376–1383.

7 Q. Li, X. H. Zhao, Q. Z. Lv and G. G. Liu, *Sep. Purif. Technol.*, 2007, **55**, 76–81.

8 Y. Liu, P. Liang and L. Guo, *Talanta*, 2005, **68**, 25–30.

9 A. A. Ensafi, T. Khayamian and A. Benvidi, *Anal. Chim. Acta*, 2006, **561**, 225–232.

10 A. P. S. Gonzales, M. A. Firmino, C. S. Nomura, F. R. P. Rocha, P. V. Oliveira and I. Gaubeur, *Anal. Chim. Acta*, 2009, **636**, 198–204.

11 (*a*) B. Naskar, R. Modak, Y. Sikdar, D. K. Maiti, A. Banik, T. K. Dangar, S. Mukhopadhyay, D. Mandal and S. Goswami, *J. Photochem. Photobiol., A*, 2016, **321**, 99–109;

(b) B. Naskar, R. Modak, D. K. Maiti, S. K. Mandal, J. K. Biswas, T. K. Mondal and S. Goswami, *Polyhedron*, 2016, **117**, 834–846; (c) B. Naskar, R. Modak, Y. Sikdar, D. K. Maiti, A. Bauzá, A. Frontera, A. Katarkar, K. Chaudhuri and S. Goswami, *Sens. Actuators, B*, 2017, **239**, 1194–1204; (d) B. Naskar, R. Modak, D. K. Maiti, A. Bauzá, A. Frontera, P. K. Maiti, S. Mandal and S. Goswami, *RSC Adv.*, 2017, **7**, 11312–11321; (e) B. Naskar, A. Dhara, R. Modak, D. K. Maiti, C. Prodhan, K. Chaudhuri, A. Requena, J. P. C. Carrasco and S. Goswami, *ChemistrySelect*, 2017, **2**, 2512–2519; (f) S. Chakraborty, C. R. Bhattacharjee, P. Mondal, S. K. Prasad and D. S. S. Rao, *Dalton Trans.*, 2015, **44**, 7477–7488; (g) K. Li and A. Tong, *Sens. Actuators, B*, 2013, **184**, 248–253; (h) F. U. Rahman, A. Ali, R. Guoa, J. Tiana, H. Wanga, Z. T. Lia and D. W. Zhang, *Sens. Actuators, B*, 2015, **211**, 544–550; (i) V. K. Gupta, A. K. Singh, L. K. Kumawat and N. Mergu, *Sens. Actuators, B*, 2016, **222**, 468–482; (j) D. Buccella, J. A. Horowitz and S. J. Lippard, *J. Am. Chem. Soc.*, 2011, **133**, 4101–4114; (k) K. Komatsu, Y. Urano, H. Kojima and T. Nagano, *J. Am. Chem. Soc.*, 2007, **129**, 13447–13454; (l) P. Du and S. J. Lippard, *Inorg. Chem.*, 2010, **49**, 10753–10755; (m) E. Tomat and S. J. Lippard, *Inorg. Chem.*, 2010, **49**, 9113–9115; (n) B. A. Wong, S. Friedle and S. J. Lippard, *Inorg. Chem.*, 2009, **48**, 7009–7011.

12 (a) R. Y. Tsien, *Fluorescent and Photochemical Probes of Dynamic Biochemical Signals inside Living Cells*, ed. A. W. Czarnik, American Chemical Society, Washington, DC, 1993, pp. 130–146; (b) Y. Xiang, A. J. Tong, P. Y. Jin and Y. Ju, *Org. Lett.*, 2006, **8**, 2863–2866.

13 A. E. Hargrove, S. Nieto, T. Zhang, J. L. Sessler and E. V. Anslyn, *Chem. Rev.*, 2011, **111**, 6603–6782.

14 J. K. Heinonen, *Biological Role of Inorganic Pyrophosphate*, Kluwer Academic Publishers, Norwell, MA, 2001.

15 (a) R. E. Wuthier, S. Bisaz, R. G. G. Russell and H. Fleisch, *Tissue Res.*, 1972, **10**, 198–206; (b) S. Q. Xu, M. He, H. P. Yu, X. K. Cai, X. L. Tan, B. Lu and B. H. Shu, *Anal. Biochem.*, 2001, **299**, 188–193.

16 (a) S. K. Kim, D. H. Lee, J. I. Hong and J. Yoon, *Acc. Chem. Res.*, 2009, **42**, 23–31; (b) S. Lee, K. K. Y. Yuen, K. A. Jolliffe and J. Yoon, *Chem. Soc. Rev.*, 2015, **44**, 1749–1762.

17 (a) L. M. Mesquita, V. André, C. V. Esteves, T. Palmeira, M. N. B. Santos, P. Mateus and R. Delgado, *Inorg. Chem.*, 2016, **55**, 2212–2219; (b) S. Anbu, S. Kamalraj, A. Paul, C. Jayabaskaran and A. J. L. Pombeiro, *Dalton Trans.*, 2015, **44**, 3930–3933; (c) Z. Hai, Y. Bao, Q. Miao, X. Yi and G. Liang, *Anal. Chem.*, 2015, **87**, 2678–2684; (d) J. H. Wang, J. B. Xiong, X. Zhang, S. Song, Z. H. Zhu and Y. S. Zheng, *RSC Adv.*, 2015, **5**, 60096–60100; (e) S. Bhowmik, B. N. Ghosh, V. Marjomaki and K. Rissanen, *J. Am. Chem. Soc.*, 2014, **136**, 5543–5546; (f) F. Huang and G. Feng, *RSC Adv.*, 2014, **4**, 484–487; (g) S. Anbu, S. Kamalraj, C. Jayabaskaran and P. S. Mukherjee, *Inorg. Chem.*, 2013, **52**, 8294–8296; (h) Q.-c. Xu, X.-f. Wang, G.-W. Xing and Y. Zhang, *RSC Adv.*, 2013, **3**, 15834–15841; (i) W. Zhu,

X. Huang, Z. Guo, X. Wu, H. Yu and H. Tian, *Chem. Commun.*, 2012, **48**, 1784–1786; (j) S. Yang, G. Feng and N. H. Williams, *Org. Biomol. Chem.*, 2012, **10**, 5606–5612; (k) B. Roy, A. S. Rao and K. H. Ahn, *Org. Biomol. Chem.*, 2011, **9**, 7774–7779; (l) I. Ravikumar and P. Ghosh, *Inorg. Chem.*, 2011, **50**, 4229–4231; (m) J. Wen, Z. Geng, Y. Yin, Z. Zhang and Z. Wang, *Dalton Trans.*, 2011, **40**, 1984–1989; (n) H. N. Lee, Z. Xu, S. K. Kim, K. M. K. Swamy, Y. Kim, S. J. Kim and J. Yoon, *J. Am. Chem. Soc.*, 2007, **129**, 3828–3829; (o) D. H. Lee, S. Y. Kim and J. I. Hong, *Angew. Chem., Int. Ed.*, 2004, **43**, 4777–4780; (p) D. H. Lee, J. H. Im, S. U. Son, Y. K. Chung and J. I. Hong, *J. Am. Chem. Soc.*, 2003, **125**, 7752–7753; (q) J. H. Lee, A. R. Jeong, J. H. Jung, C.-M. Park and J. I. Hong, *J. Org. Chem.*, 2011, **76**, 417–423; (r) W. Yu, J. Qiang, J. Yin, S. Kambam, F. Wang, Y. Wang and X. Chen, *Org. Lett.*, 2014, **16**, 2220–2223; (s) S. Svane, F. Kjeldsen, V. McKee and C. J. McKenzie, *Dalton Trans.*, 2015, **44**, 11877–11886; (t) V. E. Zwicker, B. M. Long and K. A. Jolliffe, *Org. Biomol. Chem.*, 2015, **13**, 7822–7829.

18 (a) L. Qin, J. H. Reibenspies, R. I. Carroll, A. E. Martell and A. Clearfiled, *Inorg. Chim. Acta*, 1998, **270**, 207–215; (b) D. A. Nation, A. E. Martell, R. I. Carroll and A. Clearfield, *Inorg. Chem.*, 1996, **35**, 7246–7252.

19 M. J. Frisch, G. W. Trucks, H. B. Schlegel, G. E. Scuseria, M. A. Robb, J. R. Cheeseman, G. Scalmani, V. Barone, B. Mennucci, G. A. Petersson, H. Nakatsuji, M. Caricato, X. Li, H. P. Hratchian, A. F. Izmaylov, J. Bloino, G. Zheng, J. L. Sonnenberg, M. Hada, M. Ehara, K. Toyota, R. Fukuda, J. Hasegawa, M. Ishida, T. Nakajima, Y. Honda, O. Kitao, H. Nakai, T. Vreven, J. A. Montgomery Jr., J. E. Peralta, F. Ogliaro, M. Bearpark, J. J. Heyd, E. Brothers, K. N. Kudin, V. N. Staroverov, R. Kobayashi, J. Normand, K. Raghavachari, A. Rendell, J. C. Burant, S. S. Iyengar, J. Tomasi, M. Cossi, N. Rega, J. M. Millam, M. Klene, J. E. Knox, J. B. Cross, V. Bakken, C. Adamo, J. Jaramillo, R. Gomperts, R. E. Stratmann, O. Yazyev, A. J. Austin, R. Cammi, C. Pomelli, J. W. Ochterski, R. L. Martin, K. Morokuma, V. G. Zakrzewski, G. A. Voth, P. Salvador, J. J. Dannenberg, S. Dapprich, A. D. Daniels, Ö. Farkas, J. B. Foresman, J. V. Ortiz, J. Cioslowski and D. J. Fox, *Gaussian 09, Revision C.01*, Gaussian, Inc., Wallingford CT, 2009.

20 Y. Zhao and D. G. Truhlar, *Theor. Chem. Acc.*, 2008, **120**, 215–241.

21 S. Grimme, *J. Comput. Chem.*, 2006, **27**, 1787–1799.

22 J. Tomasi, B. Mennucci and R. Cammi, *Chem. Rev.*, 2005, **105**, 2999–3094.

23 L. Zhao, J. Wu, H. Ke and J. Tang, *Inorg. Chem.*, 2014, **53**, 3519–3525.

24 T. Mosmann, *J. Immunol. Methods*, 1983, **65**, 55–63.

25 S. Hamada and S. Fujita, *Histochem. Cell Biol.*, 1983, **79**, 219–226.

26 A. Nandy, S. K. Dey, S. Das, R. N. Munda, J. Dinda and K. D. Saha, *Mol. Cancer*, 2014, **13**, 57.

27 *CrysAlis*, Oxford Diffraction Ltd, Abingdon, UK, 2006.

28 G. M. Sheldrick, *Shelxl-2016-6, Crystal Structure Refinement Program*, University of Göttingen, 2016.

29 *ABSPACK*, Oxford Diffraction Ltd, Oxford, UK, 2005.

30 (*a*) F. Habib, G. Brunet, V. Vieru, I. Korobkov, L. F. Chibotaru and M. Murugesu, *J. Am. Chem. Soc.*, 2013, **135**, 13242–13245; (*b*) G. Brunet, F. Habib, I. Korobkov and M. Murugesu, *Inorg. Chem.*, 2015, **54**, 6195–6202; (*c*) W. Dou, J. N. Yao, W. S. Liu, Y. W. Wang, J. R. Zheng and D. Q. Wang, *Inorg. Chem. Commun.*, 2007, **10**, 105–108; (*d*) F. R. Kong and M. Zhang, *Chem. J. Chin. Univ.*, 1999, **20**, 839; (*e*) J. Chakraborty, S. Thakurta, B. Samanta, A. Ray, G. Pilet, S. R. Batten, P. Jensen and S. Mitra, *Polyhedron*, 2007, **26**, 5139–5149; (*f*) L. F. Zou, L. Zhao, Y. N. Guo, J. Tang, Q. L. Wang and Y. H. Li, *Inorg. Chim. Acta*, 2012, **382**, 65–71.

31 G. J. Kleywegt, W. G. R. Wiesmeijer, G. J. V. Driel, W. L. Driessen, J. Reedijk and J. H. Noordik, *J. Chem. Soc., Dalton Trans.*, 1985, 2177–2184.

32 (*a*) A. Ruiz-Martínez, D. Casanova and S. Alvarez, *Chem. – Eur. J.*, 2008, **14**, 1291–1303; (*b*) A. Ruiz-Martínez, D. Casanova and S. Alvarez, *Dalton Trans.*, 2008, 2583–2591.

33 (*a*) C. Janiak, *J. Chem. Soc., Dalton Trans.*, 2000, 3885; (*b*) X. J. Yang, F. Drepper, B. Wu, W. H. Sun, W. Haehnel and C. Janiak, *Dalton Trans.*, 2005, 256–257; (*c*) K. Abu-Shandi, H. Winkler, H. Paulsen, R. Glaum, B. Wu and C. Janiak, *Z. Anorg. Allg. Chem.*, 2005, **631**, 2705–2714; (*d*) S. Banerjee, A. Ghosh, B. Wu, P. G. Lassahn and C. Janiak, *Polyhedron*, 2005, **24**, 593–599; (*e*) C. Zhang, G. Rheinwald, V. Lozan, B. Wu, P. G. Lassahn, H. Lang and C. Janiak, *Z. Anorg. Allg. Chem.*, 2002, **628**, 1259–1268; (*f*) E. Craven, E. Mutlu, D. Lundberg, S. Temizdemir, S. Dechert, H. Brombacher and C. Janiak, *Polyhedron*, 2002,

21, 553–562; (*g*) C. Zhang and C. Janiak, *Z. Anorg. Allg. Chem.*, 2001, **627**, 1972–1975; (*h*) C. Zhang and C. Janiak, *J. Chem. Crystallogr.*, 2001, **31**, 29–35; (*i*) M. Munakata, L. P. Wu and T. Kuroda-Sowa, *Adv. Inorg. Chem.*, 1999, **46**, 173–303.

34 (*a*) M. Nishio, *CrystEngComm*, 2004, **6**, 130–156; (*b*) M. Nishio, M. Hirota and Y. Umezawa, *The CH-Interaction*, Wiley-VCH, 1998; (*c*) Y. Umezawa, S. Tsuboyama, K. Honda, J. Uzawa and M. Nishio, *Bull. Chem. Soc. Jpn.*, 1998, **71**, 1207; (*d*) C. Janiak, S. Temizdemir, S. Dechert, W. Deck, F. Girgsdies, J. Heinze, M. J. Kolm, T. G. Scharmann and O. M. Zipffel, *Eur. J. Inorg. Chem.*, 2000, 1229; (*e*) N. N. L. Madhavi, A. K. Katz, H. L. Carrell, A. Nangia and G. R. Desiraju, *Chem. Commun.*, 1997, 1953–1954.

35 (*a*) A. Gupta and N. Kumar, *RSC Adv.*, 2016, **6**, 106413–106434; (*b*) R. Ali, S. S. Razi, P. Srivastava, M. Shahid and A. Misra, *RSC Adv.*, 2015, **5**, 61513–61520; (*c*) S. Das, M. Dutta and D. Das, *Anal. Methods*, 2013, **5**, 6262–6285; (*d*) H. Lu, W. Wang, X. Tan, X. Luo, M. Zhang, M. Zhang and S. Zang, *Dalton Trans.*, 2016, **45**, 8174–8181.

36 (*a*) M. Shortreed, R. Kopelman, M. Kuhn and B. Hoyland, *Anal. Chem.*, 1996, **68**, 1414–1418; (*b*) A. Caballero, R. Mart′ınez, V. Lloveras, I. Ratera, J. Vidal- Gancedo, K. Wurst, A. T′arraga, P. Molina and J. Veciana, *J. Am. Chem. Soc.*, 2005, **127**, 15666–15667; (*c*) W. Y. Lin, L. Yuan, Z. M. Cao, Y. M. Feng and L. Long, *Chem. – Eur. J.*, 2009, **15**, 5096–5103; (*d*) L. Rosa-Romo, M. T. Oropeza-Guzman, A. Olivas-Sarabia and G. Pina-Luis, *Sens. Actuators, B*, 2016, **233**, 459–468; (*e*) Q. Wu and E. V. Anslyn, *J. Am. Chem. Soc.*, 2004, **126**, 14682–14683; (*f*) T. Gunnlaugsson, J. P. Leonard and N. S. Murray, *Org. Lett.*, 2004, **6**, 1557–1560; (*g*) H. Qin, J. Ren, J. Wang and E. Wang, *Chem. Commun.*, 2010, **46**, 7385–7387.